Article

Production of Strange and Charm Hadrons in Pb+Pb Collisions at $\sqrt{s_{NN}} = 5.02$ TeV [†]

Wen-Bin Chang [1,2], **Rui-Qin Wang** [1], **Jun Song** [3], **Feng-Lan Shao** [1,*], **Qun Wang** [4,*] and **Zuo-Tang Liang** [5,*]

[1] School of Physics and Physical Engineering, Qufu Normal University, Qufu 273165, China
[2] Institute of Particle Physics and Key Laboratory of Quark and Lepton Physics (MOS),
   Central China Normal University, Wuhan 430079, China
[3] School of Physical Science and Intelligent Engineering, Jining University, Qufu 273155, China
[4] Department of Modern Physics, University of Science and Technology of China, Hefei 230026, China
[5] Key Laboratory of Particle Physics and Particle Irradiation (MOE), Institute of Frontier and Interdisciplinary
   Science, Shandong University, Qingdao 266237, China
* Correspondence: shaofl@mail.sdu.edu.cn (F.-L.S.); qunwang@ustc.edu.cn (Q.W.); liang@sdu.edu.cn (Z.-T.L.)
[†] This article is dedicated to the memory of Qu-bing Xie.

Abstract: Using a quark combination model with the equal-velocity combination approximation, we study the production of hadrons with strangeness and charm flavor quantum numbers in Pb+Pb collisions at $\sqrt{s_{NN}} = 5.02$ TeV. We present analytical expressions and numerical results for these hadrons' transverse momentum spectra and yield ratios. Our numerical results agree well with the experimental data available. The features of strange and charm hadron production in the quark–gluon plasma at the early stage of heavy ion collisions are also discussed.

Keywords: heavy-ion collisions; heavy-flavor production; hadronization

PACS: 27.75.-q; 25.75.Ag; 25.75.Dw; 25.75.Gz

1. Introduction

It is well-known that the hadronic matter is expected to undergo a transition to the quark–gluon plasma (QGP), a strongly coupled state of matter, at high temperatures or baryon densities [1–6]. The search for the QGP and the study of its properties have long been the goals of high-energy heavy ion collisions [7–10]. In heavy ion collisions, strange and heavy-flavor quarks are newly produced (or excited from the vacuum) and most of them are present in the whole stage of the QGP evolution. They interact strongly with the constituents of the QGP medium or they are a part of the QGP. Therefore, strange and heavy-flavor hadrons are usually regarded as special probes to the hadronization mechanism and properties of the QGP [11–22].

The relativistic heavy ion collider (RHIC) and the large hadron collider (LHC) have accumulated abundant experimental data on strange and charm hadrons [23–36]. These data show a number of features in the production of strangeness [33,34,37–40] and baryons [32,35,41–44]. Many efforts have been made to understand hadron production mechanisms in theory and phenomenology [45–62]. Hydrodynamic and thermal models [45–49] are commonly used to describe the production of strange hadrons. For the production of heavy-flavor hadrons, some transport models are popular (see, e.g., reference [63] and references therein). In particular, the coalescence or recombination models also provide good descriptions of hadron production especially at low and intermediate transverse momenta [50–56,64].

Based on Qu-Bing Xie's works in e^+e^- and pp collisions in early years [65–70], we developed a quark combination model (QCM) for hadronization and it works well in explaining yields, rapidity distributions, and transverse momentum spectra for the identified hadrons in high-energy heavy ion collisions at various energies ranging from

RHIC to LHC [53,62,71,72]. Recently, inspired by the property of constituent quark number scaling for transverse momentum spectra of strange hadrons in p+Pb collisions at LHC energy [73], we proposed a simplified version of the quark combination model by incorporating the equal-velocity combination (EVC) to replace the near rapidity combination in the original model. Many properties of hadron production can be analytically derived and some of them have been tested by experimental data in high energy pp, pA, and AA collisions [74–78]. Furthermore, our studies show that the EVC of charm and light quarks can explain the transverse momentum spectra of single-charm hadrons at low and intermediate transverse momenta [75,77–80]. In particular, the model prediction of the Λ_c^+/D^0 ratio was verified by the latest measurements of the ALICE collaboration [35,81,82].

Recently, the ALICE collaboration published precise measurements of strange and charm hadrons, especially D mesons and Λ_c^+ baryons, in Pb+Pb collisions at LHC [31,83–86]. In this paper, we apply the QCM with EVC to study the production of strange and charm hadrons simultaneously at low and intermediate transverse momenta in Pb+Pb collisions at $\sqrt{s_{NN}} = 5.02$ TeV. We will present analytical and numerical results for the p_T dependence of production ratios between different strange and charm hadrons. We will compare our results with the experimental data available and make predictions for other types of hadrons.

The rest of the paper is organized as follows. In Section 2, we introduce a general phase-space structure of the QCM in heavy ion collisions as well as the idea and formula of the QCM in momentum space based on EVC. In Sections 3 and 4, we apply the QCM to calculate spectra of various strange and charm hadrons in Pb+Pb collisions at $\sqrt{s_{NN}} = 5.02$ TeV and compare them with data. The final section is a summary of the main results and conclusions.

2. The Quark Combination Model

The QCM developed by the Shandong group led by Qu-Bing Xie [65–70] is a kind of exclusive or statistical hadronization model with constituent quarks as building blocks. A quark combination rule (QCR) can be derived for quarks and antiquarks in the neighborhood of the longitudinal phase space (momentum rapidity) to combine into baryons and mesons [65–68,87]. The QCM based on the QCR has successfully explained experimental data on hadron production in e^+e^- and pp collisions [65–70,88] as well as in heavy ion collisions [53,71,89]. A modern version of QCM with spin degrees of freedom in terms of Wigner functions has been developed by some of us and applied to spin polarization of hadrons in heavy ion collisions [90–93].

In this section, we introduce the general phase-space structure of the QCM in heavy ion collisions as well as its simplified version in momentum space to describe momentum spectra of strange and charm hadrons.

2.1. General Phase Space Structure of QCM in Heavy Ion Collisions

In the quantum kinetic theory, the formation of a composite particle through the coalescence or combination process of its constituent particles $q_1 q_2 \cdots q_n \to H$ can be described by the collision term incorporating the matrix element squared of the process and momentum integrals. In the case we are considering, the composite particle H can be a meson or a baryon, so the constituent particles $q_1 q_2 \cdots q_n$ are a quark and an antiquark for the meson, and are three quarks or three antiquarks for the baryon or antibaryon, respectively. In heavy ion collisions, the coalescence process takes place in a space-time region, i.e., the freeze-out hypersurface defined by the proper time τ_0. The momentum distribution of the hadron (meson or baryon) reads

$$f_H(\mathbf{p}) \sim \int d\sigma^\mu p_\mu \int \prod_{i=1}^n \frac{d^3\mathbf{p}_i}{(2\pi)^3 2E_i} (2\pi)^4 \delta(p_1 + p_2 + \cdots + p_n - p)$$
$$\times |M(q_1 q_2 \cdots q_n \to H)|^2 f_1(x, p_1) f_2(x, p_2) \cdots f_n(x, p_n), \tag{1}$$

where $p = (E_p, \mathbf{p})$ is the hadron's on-shell momentum, $p_i = (E_i, \mathbf{p}_i)$ is the on-shell momentum of the constituent particle q_i with its momentum distribution $f_i(x, p_i)$ at the space-time point x on the freeze-out hypersurface, M is the invariant amplitude of the coalescence process containing the hadron's wave function, and $d\sigma^\mu(x)$ is the surface element pointing to the normal direction of the freeze-out hypersurface at x. The momentum distribution can be decomposed into the thermal part and non-thermal part,

$$f_i(x, p_i) = f_i^{\text{th}}(\beta u \cdot p_i) + f_i^{\text{nth}}(p_i), \tag{2}$$

where the thermal part f_i^{th} depends on $\beta u \cdot p_i$ with $\beta(x) = 1/T(x)$ being the inverse temperature and $u^\mu(x)$ being the flow velocity both of which are functions of x on the freeze-out hypersurface, and the non-thermal part f_i^{nth} depends only on momentum and is independent of the space-time coordinate. We can express the space-time point on the freeze-out hypersurface in terms of the proper time τ and space-time rapidity η as

$$x^\mu = (\tau \cosh \eta, \mathbf{x}_T, \tau \sinh \eta), \tag{3}$$

and also the hadron's on-shell momentum in terms of transverse momentum $\mathbf{p}_T$ and rapidity Y as

$$p^\mu = (m_T \cosh Y, \mathbf{p}_T, m_T \sinh Y), \tag{4}$$

where $m_T = \sqrt{m^2 + p_T^2}$ is the transverse mass. Then the freeze-out hypersurface element can be expressed as

$$d\sigma^\mu = \tau d\eta d^2 x_T \frac{\partial x^\mu}{\partial \tau} = \tau d\eta d^2 x_T (\cosh \eta, 0, 0, \sinh \eta), \tag{5}$$

so its contraction with the hadron's momentum reads

$$d\sigma^\mu p_\mu = \tau d\eta d^2 x_T m_T \cosh(\eta - Y). \tag{6}$$

We can express the flow velocity with Bjorken's boost invariance in the longitudinal direction with $\eta = \eta_{\text{flow}}$,

$$\begin{aligned} u^\mu(x) = &[\cosh \eta \cosh \rho(x_T, \phi_s), \sinh \rho(x_T, \phi_s) \cos \phi_b, \\ &\sinh \rho(x_T, \phi_s) \sin \phi_b, \sinh \eta \cosh \rho(x_T, \phi_s)], \end{aligned} \tag{7}$$

where $\rho(x_T, \phi_s)$ is the transverse flow rapidity [94,95] as a function of cylindrical coordinates in the transverse plane $x_T = |\mathbf{x}_T|$ and ϕ_s, and ϕ_b is the boost angle in the transverse plane which can simply be taken as ϕ_s in approximation. The elliptic flow can be implemented by [95]

$$\rho(x_T, \phi_s) = \frac{x_T}{R}[\rho_0 + \rho_2 \cos(2\phi_s)], \tag{8}$$

where R is the transverse size of the fireball, and ρ_2 is linked to the elliptic flow coefficient v_2.

2.2. QCM in Momentum Space with Equal-Velocity Combination

For the purpose of this paper, we will introduce a simplified version of the QCM in momentum space with an equal-velocity combination for hadron production. This corresponds to (a) the quark distributions are homogeneous in space-time and depend only on momentum and (b) the role of the matrix element squared is taken by the EVC. This version of QCM is an approximation to the rigorous one in Section 2.1.

We consider a color-neutral system of $N_q = \sum_i N_{q_i}$ quarks and $N_{\bar{q}} = \sum_i N_{\bar{q}_i}$ antiquarks where $q_i = u, d, s, c$ and $\bar{q}_i = \bar{u}, \bar{d}, \bar{s}, \bar{c}$ denote the quark and antiquark flavors, respectively. The momentum distributions $f_{M_j}(p) \equiv f_{M_j}(p; N_q, N_{\bar{q}})$ and $f_{B_j}(p) \equiv f_{B_j}(p; N_q, N_{\bar{q}})$ for the

directly produced meson M_j and baryon B_j by combining a pair of quark–antiquarks and three quarks, respectively, can be schematically expressed as

$$f_{M_j}(p) = \sum_{\bar{q}_1 q_2} \int dp_1 dp_2 N_{\bar{q}_1 q_2} f_{\bar{q}_1 q_2}^{(n)}(p_1, p_2) \mathcal{R}_{M_j, \bar{q}_1 q_2}(p; p_1, p_2), \tag{9}$$

$$f_{B_j}(p) = \sum_{q_1 q_2 q_3} \int dp_1 dp_2 dp_3 N_{q_1 q_2 q_3} f_{q_1 q_2 q_3}^{(n)}(p_1, p_2, p_3) \mathcal{R}_{B_j, q_1 q_2 q_3}(p; p_1, p_2, p_3), \tag{10}$$

where $f_{\bar{q}_1 q_2}^{(n)}$ and $f_{q_1 q_2 q_3}^{(n)}$ are normalized joint momentum distributions; $N_{\bar{q}_1 q_2}$ and $N_{q_1 q_2 q_3}$ are the number of $\bar{q}_1 q_2$ pairs and that of $q_1 q_2 q_3$ clusters in the system; $\mathcal{R}_{M_j, \bar{q}_1 q_2}$ and $\mathcal{R}_{B_j, q_1 q_2 q_3}$ are combination kernel functions that stand for the probability density for a $\bar{q}_1 q_2$ pair with momenta p_1 and p_2 to combine into a meson M_j of momentum p and that for a $q_1 q_2 q_3$ cluster with p_1, p_2, and p_3 to combine into a baryon B_j of momentum p, respectively.

Just as derived in Refs. [75,76], the combination kernel functions in the EVC can be written as

$$\mathcal{R}_{M_j, \bar{q}_1 q_2}(p; p_1, p_2) = C_{M_j} \mathcal{R}_{\bar{q}_1 q_2}^{(f)} \mathcal{A}_{M, \bar{q}_1 q_2} \delta(p_1 - x_{q_1 q_2}^{q_1} p) \delta(p_2 - x_{q_1 q_2}^{q_2} p), \tag{11}$$

$$\mathcal{R}_{B_j, q_1 q_2 q_3}(p; p_1, p_2, p_3) = C_{B_j} \mathcal{R}_{q_1 q_2 q_3}^{(f)} \mathcal{A}_{B, q_1 q_2 q_3} \delta(p_1 - x_{q_1 q_2 q_3}^{q_1} p)$$
$$\times \delta(p_2 - x_{q_1 q_2 q_3}^{q_2} p) \delta(p_3 - x_{q_1 q_2 q_3}^{q_3} p), \tag{12}$$

where δ-functions guarantee the momentum conservation in the EVC and $x_{q_1 q_2}^{q_i} = m_{q_i}/(m_{q_1} + m_{q_2})$ and $x_{q_1 q_2 q_3}^{q_i} = m_{q_i}/(m_{q_1} + m_{q_2} + m_{q_3})$ are the momentum fraction of the produced hadron for q_i. We note that the mass fraction is the same as the momentum fraction in the EVC. Masses of up, down, strange, and charm quarks are taken to be $m_u = m_d = 0.3$ GeV, $m_s = 0.5$ GeV and $m_c = 1.5$ GeV, respectively.

The factor C_{M_j} is the probability for M to be M_j if the quark content of M is the same as M_j and similar for C_{B_j}. In this paper, we only consider hadrons in the ground state, namely mesons with $J^P = 0^-$ and 1^- and baryons with $J^P = (1/2)^+$ and $(3/2)^+$. In this case, C_{M_j} is the same for all hadrons in the same multiplet (with the same J^P) and determined by the production ratio of vector to pseudo-scalar mesons $R_{V/P}$, so is it for C_{B_j} which is determined by the production ratio of $J^P = (1/2)^+$ to $J^P = (3/2)^+$ baryons $R_{O/D}$ with the same flavor content.

The factors $\mathcal{R}_{\bar{q}_1 q_2}^{(f)}$ and $\mathcal{R}_{q_1 q_2 q_3}^{(f)}$ contain Kronecker δ's to guarantee the quark flavor conservation, e.g., if M_j is a D-meson with constituent quark content $\bar{q}c$, $\mathcal{R}_{\bar{q}_1 q_2}^{(f)} = \delta_{q_1, q} \delta_{q_2, c}$. If B_j is a single-charm baryon with the quark content udc, $\mathcal{R}_{q_1 q_2 q_3}^{(f)} = N_{\text{sym}} \delta_{q_1, u} \delta_{q_2, d} \delta_{q_3, c}$, where $N_{\text{sym}} = 1, 3, 6$ is a symmetry factor to account for the number of different permutations of three quarks for (a) three identical flavors, (b) two identical flavors, and (c) all three distinct flavors, respectively.

The factor $\mathcal{A}_{M, \bar{q}_1 q_2}$ is the probability for a quark q_2 to capture a specific antiquark $\bar{q}_1$ to form a meson in the quark–antiquark system; it should be inversely proportional to $N_q + N_{\bar{q}}$. Similarly, $\mathcal{A}_{B, q_1 q_2 q_3}$ should be inversely proportional to $(N_q + N_{\bar{q}})^2$. Both $\mathcal{A}_{M, \bar{q}_1 q_2}$ and $\mathcal{A}_{B, q_1 q_2 q_3}$ are determined by the unitarity and the competition mechanism of meson-baryon production. Note that for light-quark systems produced in $e^+ e^-$ and pp collisions, $\mathcal{A}_{M, \bar{q}_1 q_2}$ and $\mathcal{A}_{B, q_1 q_2 q_3}$ correspond to combination weights of mesons and baryons that follow the QCR [65,66,87].

Putting all these factors together, for charm hadrons we are considering, Equations (9) and (10) become

$$f_{M_j}(p) = \frac{N_c N_{\bar{q}_1}}{N_q + N_{\bar{q}}} \mathcal{A}_M C_{M_j} f_{\bar{q}_1 c}^{(n)}(x_{q_1 c}^{q_1} p, x_{q_1 c}^c p), \tag{13}$$

$$f_{B_j}(p) = \frac{N_c N_{q_1} N_{q_2}}{(N_q + N_{\bar{q}})^2} \mathcal{A}_B C_{B_j} N_{\text{sym}} f_{q_1 q_2 c}^{(n)}(x_{q_1 q_2 c}^{q_1} p, x_{q_1 q_2 c}^{q_2} p, x_{q_1 q_2 c}^c p), \tag{14}$$

where $\mathcal{A}_M$ and $\mathcal{A}_B$ are two global coefficients that can be determined by quark number conservation in the combination process and the baryon-to-meson production ratio N_B/N_M. We are considering a quark–antiquark system in the mid-rapidity region at very high collision energies, so that net baryon number and net quark flavor are negligible, i.e., $N_{\bar{q}_i} \approx N_{q_i}$ for $i = u, d, s, c$. Moreover, we assume that the number of strange quarks is suppressed by a factor λ_s (strangeness suppression factor) relative to that of up and down quarks, so we have $N_u : N_d : N_s = 1 : 1 : \lambda_s$.

If we neglect correlations in the joint momentum distributions among different momenta, we have factorization forms for the joint momentum distributions,

$$f_{\bar{q}_1 q_2}^{(n)}(p_1, p_2) = f_{\bar{q}_1}^{(n)}(p_1) f_{q_2}^{(n)}(p_2), \tag{15}$$

$$f_{q_1 q_2 q_3}^{(n)}(p_1, p_2, p_3) = f_{q_1}^{(n)}(p_1) f_{q_2}^{(n)}(p_2) f_{q_3}^{(n)}(p_3). \tag{16}$$

We will use the above factorization forms in Equations (13) and (14) in our numerical calculation for single-charm hadrons. By using Equations (13) and (14) with Equations (15) and (16), we are able to calculate momentum spectra and yields for different hadrons.

Including strong and electromagnetic decay contributions from short-lived resonances [96], we can obtain the momentum spectra of final state hadrons and make comparison with experimental data. For charm hadrons, we make an approximation that the momentum of the daughter charm hadron is almost equal to that of the mother charm hadron. With this approximation and the production ratio of the vector to the pseudo-scalar meson being set to 1.5 [28,80], we obtain (for the final state D mesons):

$$f_{D^0}^{(\mathrm{fin})}(p) \approx 3.516 f_{D^0}(p), \tag{17}$$

$$f_{D^+}^{(\mathrm{fin})}(p) \approx 1.485 f_{D^+}(p), \tag{18}$$

$$f_{D_s^+}^{(\mathrm{fin})}(p) \approx 2.5 f_{D_s^+}(p). \tag{19}$$

Similarly, we can set the production ratio of $J^P = (1/2)^+$ to the $J^P = (3/2)^+$ single-charm baryon to 2 [80] and obtain,

$$f_{\Lambda_c^+}^{(\mathrm{fin})}(p) \approx 5 f_{\Lambda_c^+}(p), \tag{20}$$

$$f_{\Sigma_c^0}^{(\mathrm{fin})}(p) \approx f_{\Sigma_c^0}(p), \tag{21}$$

$$f_{\Sigma_c^+}^{(\mathrm{fin})}(p) \approx f_{\Sigma_c^+}(p), \tag{22}$$

$$f_{\Sigma_c^{++}}^{(\mathrm{fin})}(p) \approx f_{\Sigma_c^{++}}(p), \tag{23}$$

$$f_{\Xi_c^0}^{(\mathrm{fin})}(p) \approx 2.5 f_{\Xi_c^0}(p), \tag{24}$$

$$f_{\Xi_c^+}^{(\mathrm{fin})}(p) \approx 2.5 f_{\Xi_c^+}(p), \tag{25}$$

$$f_{\Omega_c^0}^{(\mathrm{fin})}(p) \approx 1.5 f_{\Omega_c^0}(p). \tag{26}$$

These analytical results can be used to obtain the p_T spectra of charm hadrons. For final state strange hadrons, there are no such analytical results, only numerical ones.

3. Transverse Momentum Spectra and Baryon-to-Meson Ratio for Strange Hadrons

In this section, we apply the QCM introduced in Section 2 to study the production of strange hadrons in Pb+Pb collisions at $\sqrt{s_{NN}} = 5.02$ TeV. We first calculate the p_T spectra of strange mesons and baryons. Then we calculate the baryon-to-meson ratio Λ/K_s^0 as a function of p_T in different types of centralities.

3.1. Transverse Momentum Spectra of Strange Hadrons

The inputs of the model are p_T spectra of quarks and antiquarks. In this paper, we adopt the isospin symmetry and neglect the net quark numbers ($N_{q_i} \approx N_{\bar{q}_i}$ for $i = u, d, s, c$) in the mid-rapidity region at LHC energy, so we have only two inputs $f_d(p_T) = f_u(p_T)$ and $f_s(p_T)$, which can be fixed by fitting the experimental data on the p_T spectra of ϕ mesons and Λ baryons [40,97,98]. The extracted results for the normalized p_T spectra of quarks in central 0–5% to peripheral 70–80% Pb+Pb collisions at $\sqrt{s_{NN}} = 5.02$ TeV are shown in Figure 1. The rapidity densities of d and s quarks are listed in Table 1.
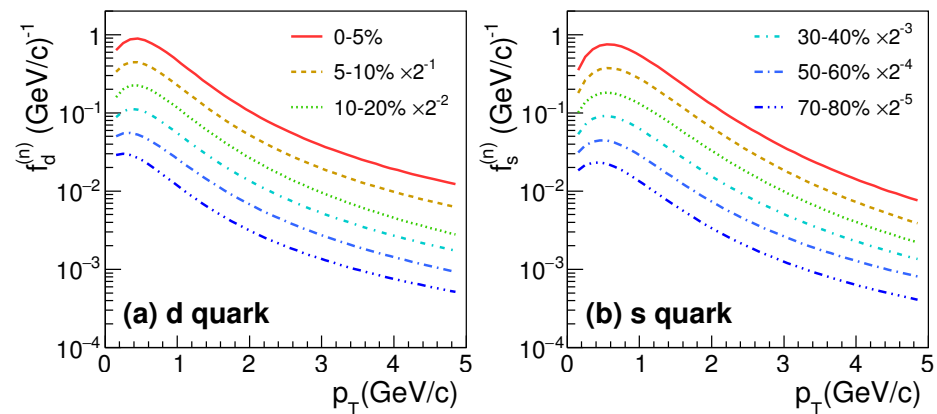

Figure 1. The normalized p_T distributions of (**a**) d quark and (**b**) s quark in different centralities in Pb+Pb collisions at $\sqrt{s_{NN}} = 5.02$ TeV.

Table 1. Rapidity densities of d and s quarks in different centralities in Pb+Pb collisions at $\sqrt{s_{NN}} = 5.02$ TeV.

Centrality	dN_d/dy	dN_s/dy
0–5%	840	370
5–10%	686	302
10–20%	516	227
30–40%	267	115
50–60%	97	40
70–80%	27	10

In Figure 2, we show the results for the p_T spectra of K_s^0 and Λ in 0–5%, 5–10%, 10–20%, 30–40%, 50–60%, 70–80% centralities, and those of ϕ, Ξ^- and Ω^- in 0–10%, 10–20%, 30–40%, 50–60%, 70–80% centralities. The QCM results are displayed in lines and experimental data [97,98] are displayed in open symbols. From Figure 2, we see that our QCM results for strange mesons and baryons agree with the experimental data very well. Such a good agreement provides a piece of evidence for the EVC mechanism in describing strange hadron production in Pb+Pb collisions at the LHC energy.
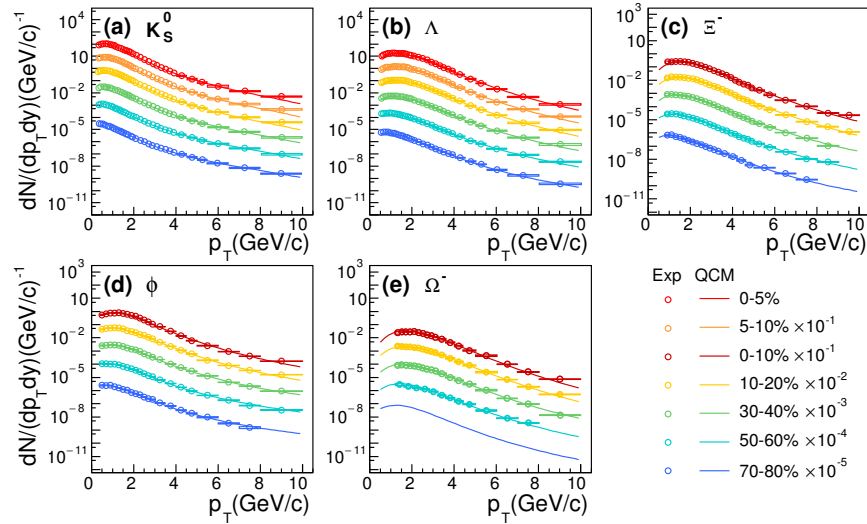
Figure 2. The p_T spectra of (**a**) K_s^0, (**b**) Λ, (**c**) Ξ^-, (**d**) ϕ and (**e**) Ω^- in different centralities in Pb+Pb collisions at $\sqrt{s_{NN}} = 5.02$ TeV. Open symbols are experimental data [97,98]. Lines for Λ and ϕ are fitting results that are used to fix p_T spectra of light-flavor quarks at hadronization in QCM. Lines for K_S^0, Ξ^- and Ω^- are predictions from QCM.

3.2. Baryon-To-Meson Ratio Λ/K_S^0

Figure 3 shows the multiplicity ratio Λ/K_S^0 as a function of p_T in five centrality ranges 0–5%, 10–20%, 30–40%, 50–60%, and 70–80%. Filled squares are experimental data [98], and lines are the QCM results. We see that Λ/K_S^0 exhibits an increase-peak-decrease behavior as a function of p_T in all centralities, which is regarded as a natural consequence of quark recombination [50–52,99,100]. We see that this feature can be well described by the QCM with EVC. The height of the peak increases from about 0.8 in the peripheral (70–80% centrality) to about 1.5 in the most central (0-5% centrality) collisions. The peak positions in the p_T slightly move to higher values from peripheral to central collisions due to stronger radial flows in more central collisions. The QCM with EVC gives a good description of the p_T dependence of Λ/K_S^0.
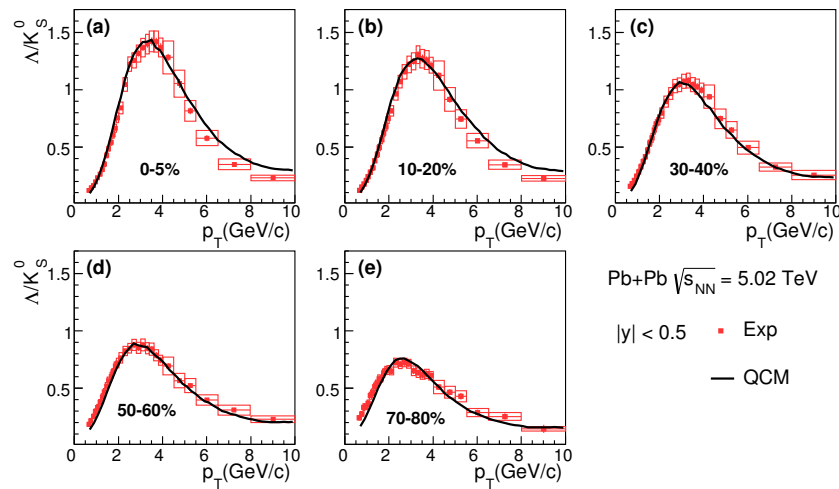

Figure 3. The p_T dependence of Λ/K_S^0 in (**a**) 0–5%, (**b**) 10–20%, (**c**) 30–40%, (**d**) 50–60%, (**e**) 70–80% centralities in Pb+Pb collisions at $\sqrt{s_{NN}} = 5.02$ TeV. Filled squares are experimental data [98] and lines are the QCM results.

4. Transverse Momentum Spectra, Yield Ratios, and Nuclear Modification Factor for Charm Hadrons

In this section, we apply the QCM with EVC to study the production of charm hadrons at midrapidity in Pb+Pb collisions at $\sqrt{s_{NN}} = 5.02$ TeV. We first calculate the p_T spectra of D mesons and single-charm baryons. Then we give the p_T dependence of yield ratios of different charm hadrons. Finally, we give the nuclear modification factor R_{AA} for charm hadrons as a function of p_T.

4.1. Transverse Momentum Spectra of Charm Mesons and Baryons

In the QCM, the only additional input is the normalized p_T distribution of the charm quarks, which we adopt a hybrid form based on the simulation of charm quarks propagating in the QGP medium in a Boltzmann transport approach [100,101]

$$f_c^{(n)}(p_T) = \frac{1}{N_{\text{norm}}} p_T \left[\left(\frac{p_T}{p_{T0}} \right)^{\alpha_c} \exp\left(-\frac{\sqrt{p_T^2 + m_c^2}}{T_c} \right) + \left(1.0 + \frac{\sqrt{p_T^2 + m_c^2} - m_c}{\Gamma_c} \right)^{-\beta_c} \right]. \quad (27)$$

At small p_T, this parameterized form is very close to the thermal distribution, while at large p_T, it follows the power law which is a non-thermal distribution. Both the thermal and non-thermal distributions are smoothly connected through the above parameterization. Here, the normalization constant N_{norm} can be determined by the condition $\int_0^\infty dp_T f_c^{(n)}(p_T) = 1$. The parameters α_c, p_{T0}, T_c, Γ_c, and β_c are fitted using the data of D^0's p_T spectra [31,84] and are listed in Table 2. The shapes of $f_c^{(n)}(p_T)$ at different centralities are shown in Figure 4a. We see that there is a stronger suppression in more central collisions in the p_T range 4 GeV $< p_T <$ 10 GeV. Figure 4b shows $f_c^{(n)}(p_T)$ at different centralities normalized by 60–80% centrality, which has similar behavior to the nuclear modification factor R_{CP} of the D^0 meson measured in reference [31]. For the rapidity density of charm quarks dN_c/dy, we assume that it is proportional to the cross-section per rapidity in pp collisions as

$$\frac{dN_c}{dy} = \langle T_{AA} \rangle \frac{d\sigma_c^{\text{pp}}}{dy}. \quad (28)$$

Here, $\langle T_{AA} \rangle$ is the average nuclear overlap function [31], $d\sigma_c^{pp}/dy$ is the p_T integrated cross-section of charm quarks in pp collisions which is about 1.0 mb at $\sqrt{s} = 5.02$ TeV [77]. The values of dN_c/dy at different centralities are listed in Table 2.
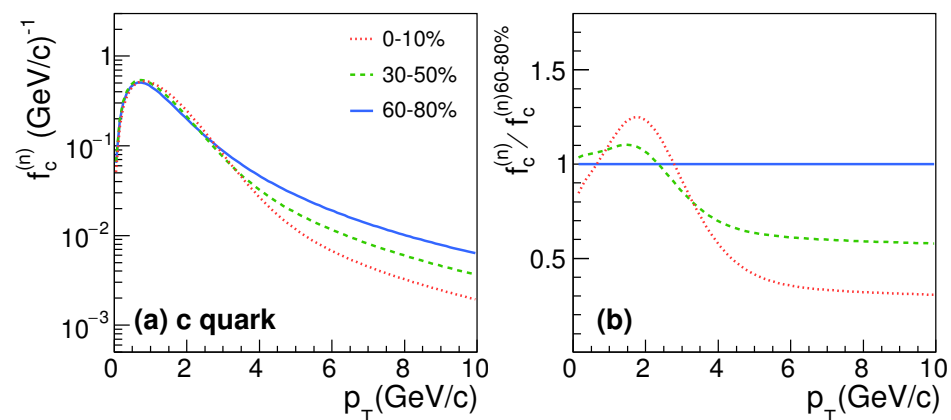

Figure 4. (**a**) Normalized p_T distribution of the charm quarks $f_c^{(n)}(p_T)$ at different centralities. (**b**) The distribution $f_c^{(n)}(p_T)$ at different centralities normalized by that at 60–80% centrality.

Table 2. The parameters in the normalized p_T distribution of the charm quarks at different centralities.

Centrality	0–10%	30–50%	60–80%
p_{T0} (GeV/c)	0.0051	0.10	0.63
α_c	0.5	1.0	1.5
T_c (GeV)	0.46	0.38	0.34
β_c	3.10	3.00	2.95
Γ_c (GeV)	0.6	0.6	0.7
dN_c/dy	23.07	3.90	0.417

In Figure 5, we present the results for the p_T spectra of D^0, D^+, D_s^+, and D^{*+} mesons at 0–10%, 30–50%, and 60–80% centralities. Open symbols are the experimental data [31,84,85] and lines are the calculated results. The results agree with the experimental data in the p_T range from 0.5 GeV/c up to 10 GeV/c.

Figure 6 shows the results for charm baryons at 0–10%, 30–50%, and 60–80% centralities. Open symbols [only in Figure 6a] are the data of Λ_c^+ [86] and lines are the results from the QCM, which are in good agreement. Predictions from QCM for other charm baryons Σ_c^0, Ξ_c^+, and Ω_c^0 are presented in Figure 6b–d, which can be tested in future experimental measurements.

The agreement between our results and experimental data for various D mesons and Λ_c^+ baryons indicates the validity of the EVC mechanism in the QCM in describing the charm hadron production. In this mechanism, the formation of the charm hadron is through the capture of light quarks in the medium by the charm quark with the same velocity.
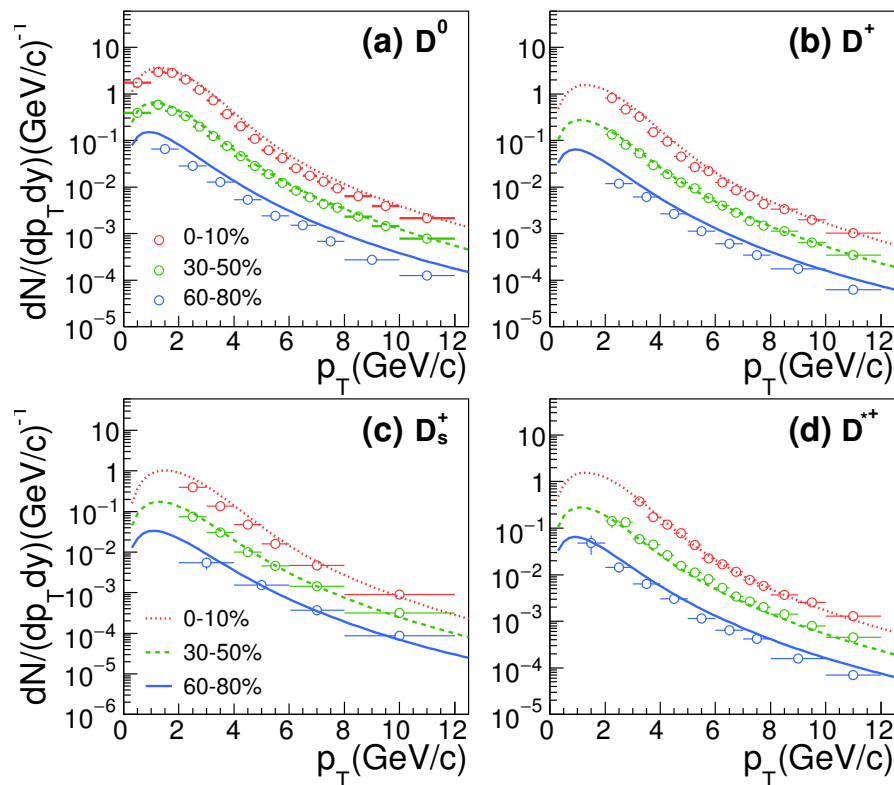

Figure 5. The p_T spectra of (**a**) D^0, (**b**) D^+, (**c**) D_s^+, and (**d**) D^{*+} mesons at different centralities. Open symbols are the experimental data [31,84,85]. Lines for D^0 are fitting results that are used to fix the shape parameters in the p_T spectrum of charm quarks at hadronization in Equation (27). Lines for D^+, D_s^+ and D^{*+} are predictions from QCM.
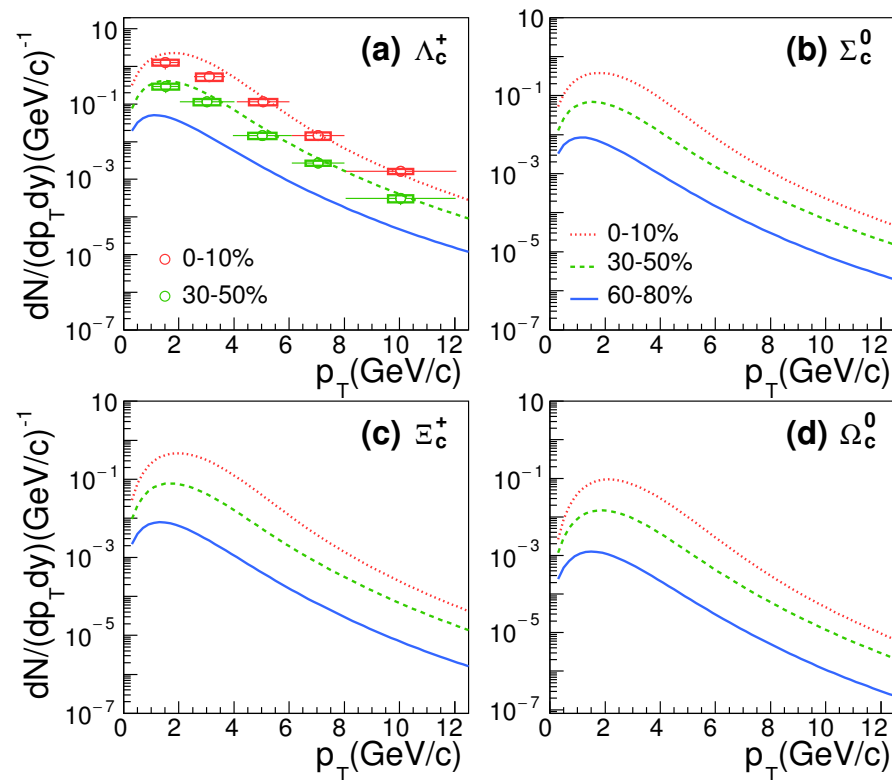
Figure 6. The p_T spectra of (**a**) Λ_c^+, (**b**) Σ_c^0, (**c**) Ξ_c^+, and (**d**) Ω_c^0 baryons at different centralities. Open symbols are the data of Λ_c^+ [86], and lines are the QCM results.

We also calculated p_T-integrated yield density dN/dy for charm hadrons at midrapidity and 0–10%, 30–50%, and 60–80% centralities as listed in Table 3. The experimental data are taken from Refs. [84,85]. The QCM results are slightly higher than data. This is because we only include single-charm hadrons in the calculation and assume all charm quarks go to single-charm hadrons. In fact, the hidden-charm J/Ψ, double-charm baryons, and even heavy-flavor multiquark states can be produced. If including these particles, our results in Table 3 will decrease slightly and the agreement with experimental data will be improved. No data are available for the yield densities of many charm hadrons; our QCM predictions can be tested by their future experimental measurements.

Table 3. The yield density dN/dy for charm hadrons at different centralities. The experimental data are from Refs. [84,85].

Hadron	0–10%		30–50%		60–80%	
	Data	QCM	Data	QCM	Data	QCM
D^0	$6.819 \pm 0.457^{+0.912}_{-0.936} \pm 0.054$	8.438	$1.275 \pm 0.099^{+0.167}_{-0.173} \pm 0.010$	1.436	—	0.157
D^+	$3.041 \pm 0.073^{+0.154}_{-0.155} \pm 0.052^{+0.352}_{-0.618}$	3.563	$0.552 \pm 0.008^{+0.024}_{-0.024} \pm 0.009^{+0.068}_{-0.114}$	0.606	—	0.0665
D^{*+}	$3.803 \pm 0.037^{+0.084}_{-0.085} \pm 0.041^{+0.854}_{-1.175}$	3.600	$0.663 \pm 0.023^{+0.038}_{-0.039} \pm 0.007^{+0.149}_{-0.165}$	0.613	—	0.0672
D_s^+	$1.89 \pm 0.07^{+0.13+0.36}_{-0.16-0.55} \pm 0.07$	2.417	$0.34 \pm 0.01^{+0.02+0.11}_{-0.03-0.09} \pm 0.01$	0.395	—	0.0368
Λ_c^+	—	5.983	—	1.026	—	0.115
Σ_c^0	—	0.997	—	0.171	—	0.0192
Σ_c^{++}	—	0.997	—	0.171	—	0.0192
Ξ_c^0	—	1.211	—	0.199	—	0.0189
Ξ_c^+	—	1.211	—	0.199	—	0.0189
Ω_c^0	—	0.246	—	0.0386	—	0.00311

4.2. Yield Ratios for Charm Hadrons

In this subsection, we calculate two kinds of yield ratios as functions of p_T for charm hadrons: one is D_s^+/D^0 which is related to strangeness production, and the other is the baryon-to-meson ratio.

We first look at the results for D_s^+/D^0 in Figure 7 at 0–10%, 30–50% and 60–80% centralities. The symbols in panels (a) and (b) are from the most recent data [85], while those in panel (c) are from previous measurements [31]. Different lines are the QCM results. The agreement between the data and our results with the same value of λ_s extracted from strange hadrons implies the same 'strangeness' environment for both strange and charm hadrons and supports the QCM works as the hadronization mechanism for charm quarks in the QGP medium.
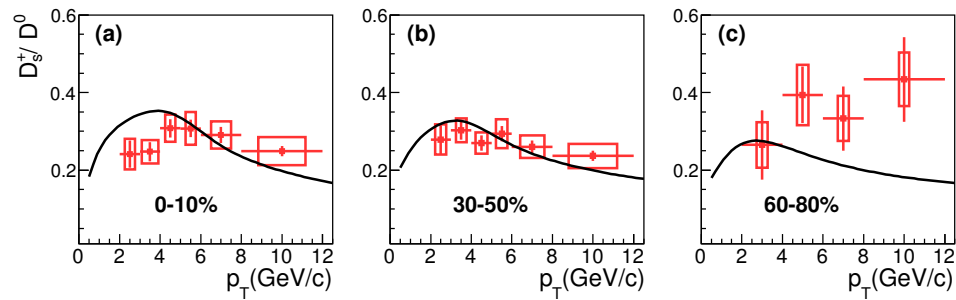
Figure 7. D_s^+/D^0 as a function of p_T for (**a**) 0–10%, (**b**) 30–50%, and (**c**) 60–80% centralities. The symbols are experimental data [31,85], and solid lines are the QCM results.

We then look at the baryon-to-meson ratio Λ_c^+/D^0, which is considered a probe to the charm quark hadronization. Recalling Equations (17,20), we have

$$\frac{\Lambda_c^+}{D^0} = \frac{4.267}{2+\lambda_s} \cdot \frac{\mathcal{A}_B}{\mathcal{A}_M} \cdot \frac{[f_d^{(n)}(x_{ddc}^d p_T)]^2 f_c^{(n)}(x_{ddc}^c p_T)}{f_d^{(n)}(x_{dc}^d p_T) f_c^{(n)}(x_{dc}^c p_T)} .$$ (29)

In our calculation, we set $\mathcal{A}_B/\mathcal{A}_M$ to 0.45 by $R_{B/M} = 0.6$ in the charm sector [75]. Following Equation (29), the results for Λ_c^+/D^0 as a function of p_T at different centralities are given in Figure 8. We see that Λ_c^+/D^0 as a function of p_T shows a similar shape to Λ/K_S^0 in Figure 3 except a larger shift in the p_T at the peak value from the central to peripheral collisions; in the central to peripheral collisions, the peak values decrease from about 1.3 to 0.9 and their locations in the p_T shift from 5 to 3 GeV. The peak locations shifting lower p_T from the central to peripheral collisions is due to the stronger collectivity in more central collisions.
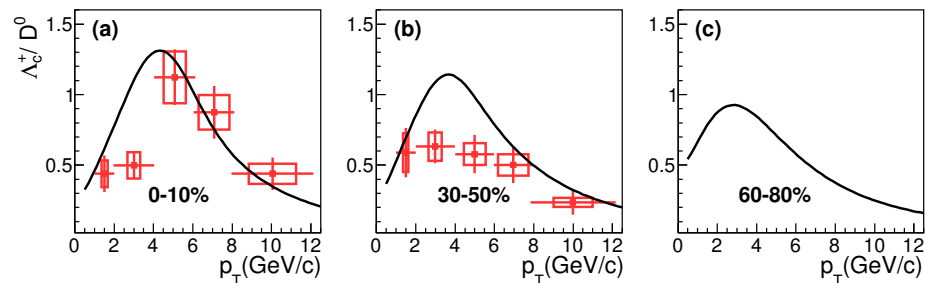

Figure 8. The baryon-to-meson ratio Λ_c^+/D^0 as a function of p_T for (**a**) 0–10%, (**b**) 30–50%, and (**c**) 60–80% centralities. Symbols are experimental data [86], and solid lines are the QCM results.

4.3. Nuclear Modification Factor R_{AA}

We finally investigate the nuclear modification factor R_{AA} for charm hadrons, which is defined as

$$R_{AA}(p_T) = \frac{1}{\langle T_{AA} \rangle} \frac{dN_{AA}/dp_T}{d\sigma_{pp}/dp_T}. \tag{30}$$

The results for differential cross-sections of charm hadrons in *pp* collisions at $\sqrt{s} = 5.02$ TeV are taken from reference [77] by some of us. Figure 9 shows R_{AA} for prompt D^0, D^+ and D^{*+} mesons as well as Λ_c^+ at 0–10% and 30–50% centralities. Symbols are experimental data [84,86], and solid lines are the QCM results. One can see in Figure 9 that both D mesons and Λ_c^+ have similar p_T behaviors. The peaks are located at p_T^{peak} which shifts towards higher values from peripheral to central collisions. This shift is mainly due to the stronger collectivity in central collisions which can boost thermal quarks to larger transverse momenta that are passed to charm hadrons by the EVC mechanism. We also see that the peak shift for R_{AA} of Λ_c^+ is more obvious than that of D mesons, because Λ_c^+ contains two light quarks and therefore is more influenced by centrality-dependent collectivity.
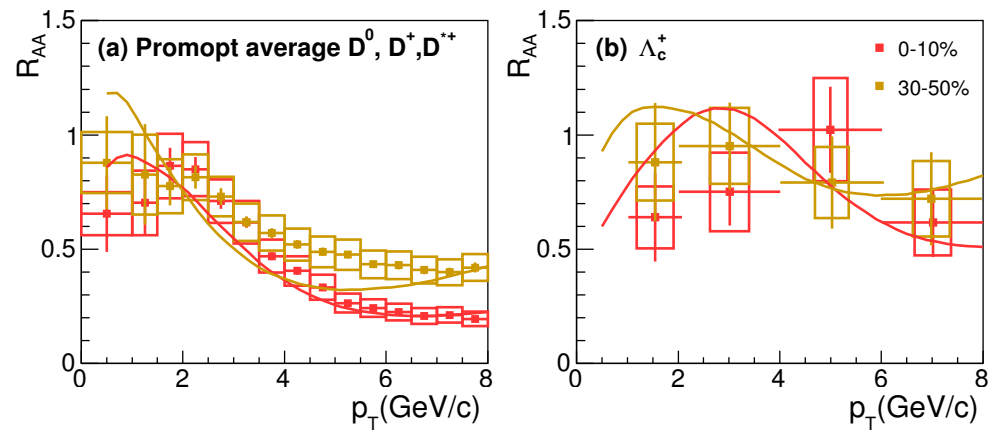

Figure 9. The nuclear modification factor R_{AA} for (**a**) prompt D^0, D^+ and D^{*+} mesons and (**b**) Λ_c^+ baryons as functions of p_T at different centralities. Symbols are experimental data from Refs. [84,86], and solid lines are the QCM results.

5. Summary

The comparative study of the production properties of strange and charm hadrons can provide information on the hadronization mechanism in relativistic heavy ion collisions. We use a quark combination model in momentum space with the approximation of equal-velocity combination to study these properties in Pb+Pb collisions at $\sqrt{s_{NN}} = 5.02$ TeV. We used experimental data of Λ, ϕ and D^0 to fix the p_T spectra of up, strange, and charm quarks at hadronization. We computed the p_T spectra and rapidity densities of K_s^0, Ξ^-, Ω^-, D^+, D_s^+, D^{*+}, Λ_c^+, Σ_c^0, Ξ_c^+ and Ω_c^0 from central to peripheral collisions. The QCM results agree with the available experimental data quite well.

We calculated the yield ratios Λ/K_S^0, D_s^+/D^0 and Λ_c^+/D^0 as functions of p_T. We found that the EVC-based QCM in momentum space can naturally describe their non-trivial behaviors as functions of the p_T and the centrality. The p_T locations of the peaks in these ratio curves shift to lower values from central to peripheral collisions, an effect arising from collectivity in heavy ion collisions, absent in pp collisions. The calculated results for the nuclear modification factor R_{AA} show similar behaviors for both D and Λ_c^+, which can be tested by more precise experimental measurements, especially at a low p_T. All our results support the validity of the EVC-based QCM in describing the hadronization mechanism of charm quarks in high energy heavy ion collisions.

References

1. Shuryak, E.V. Quantum Chromodynamics and the Theory of Superdense Matter. *Phys. Rept.* **1980**, *61*, 71–158. [CrossRef]
2. Braun-Munzinger, P.; Wambach, J. The Phase Diagram of Strongly-Interacting Matter. *Rev. Mod. Phys.* **2009**, *81*, 1031–1050. [CrossRef]
3. Fukushima, K.; Hatsuda, T. The phase diagram of dense QCD. *Rept. Prog. Phys.* **2011**, *74*, 014001. [CrossRef]
4. Borsanyi, S.; Fodor, Z.; Hoelbling, C.; Katz, S.D.; Krieg, S.; Ratti, C.; Szabo, K.K. Is there still any T_c mystery in lattice QCD? Results with physical masses in the continuum limit III. *JHEP* **2010**, *09*, 073. [CrossRef]
5. Bazavov, A.; Bhattacharya, T.; Cheng, M.; DeTar, C.; Ding, H.-T.; Gottlieb, S.; Gupta, R.; Hegde, P.; Heller, U.M.; Karsch, F.; et al. The chiral and deconfinement aspects of the QCD transition. *Phys. Rev. D* **2012**, *85*, 054503. [CrossRef]
6. Ding, H.T.; Karsch, F.; Mukherjee, S. Thermodynamics of strong-interaction matter from Lattice QCD. *Int. J. Mod. Phys. E* **2015**, *24*, 1530007. [CrossRef]
7. Adams, J.; Aggarwal, M.M.; Ahammed, Z.; Amonett, J.; Anderson, B.D.; Arkhipkin, D.; Averichev, G.S.; Badyal, S.K.; Bai, Y.; Balewski, J.; et al. Experimental and theoretical challenges in the search for the quark gluon plasma: The STAR Collaboration's critical assessment of the evidence from RHIC collisions. *Nucl. Phys. A* **2005**, *757*, 102–183. [CrossRef]
8. Adcox, K.; Adler, S.S.; Afanasiev, S.; Aidala, C.; Ajitanand, N.N.; Akiba, Y.; Al-Jamel, A.; Alexander, J.; Amirikas, R.; Aoki, K.; et al. Formation of dense partonic matter in relativistic nucleus-nucleus collisions at RHIC: Experimental evaluation by the PHENIX collaboration. *Nucl. Phys. A* **2005**, *757*, 184–283. [CrossRef]
9. Back, B.B.; Baker, M.D.; Ballintijn, M.; Barton, D.S.; Becker, B.; Betts, R.R.; Bickley, A.A.; Bindel, R.; Budzanowski, A.; Busza, W.; et al. The PHOBOS perspective on discoveries at RHIC. *Nucl. Phys. A* **2005**, *757*, 28–101. [CrossRef]
10. Arsene, I.; Bearden, I.G.; Beavis, D.; Besliu, C.; Budick, B.; Boggild, H.; Chasman, C.; Christensen, C.H.; Christiansen, P.; Cibor, J.; et al. Quark gluon plasma and color glass condensate at RHIC? The Perspective from the BRAHMS experiment. *Nucl. Phys. A* **2005**, *757*, 1–27. [CrossRef]
11. Rafelski, J.; Muller, B. Strangeness Production in the Quark-Gluon Plasma. *Phys. Rev. Lett.* **1986**, *48*, 1066. Erratum in *Phys. Rev. Lett.* **1986**, *56*, 2334. [CrossRef]
12. Shor, A. Phi meson production as a probe of the quark gluon plasma. *Phys. Rev. Lett.* **1985**, *54*, 1122–1125. [CrossRef] [PubMed]
13. van Hecke, H.; Sorge, H.; Xu, N. Evidence of early multistrange hadron freezeout in high-energy nuclear collisions. *Phys. Rev. Lett.* **1998**, *81*, 5764–5767. [CrossRef]
14. Matsui, T.; Satz, H. J/ψ Suppression by Quark-Gluon Plasma Formation. *Phys. Lett. B* **1986**, *178*, 416–422. [CrossRef]
15. van Hees, H.; Greco, V.; Rapp, R. Heavy-quark probes of the quark-gluon plasma at RHIC. *Phys. Rev. C* **2006**, *73*, 034913. [CrossRef]
16. Mocsy, A.; Petreczky, P. Color screening melts quarkonium. *Phys. Rev. Lett.* **2007**, *99*, 211602. [CrossRef]
17. He, M.; Fries, R.J.; Rapp, R. D_s-Meson as Quantitative Probe of Diffusion and Hadronization in Nuclear Collisions. *Phys. Rev. Lett.* **2013**, *110*, 112301. [CrossRef]
18. Braun-Munzinger, P.; Koch, V.; Schäfer, T.; Stachel, J. Properties of hot and dense matter from relativistic heavy ion collisions. *Phys. Rept.* **2016**, *621*, 76–126. [CrossRef]
19. Batsouli, S.; Kelly, S.; Gyulassy, M.; Nagle, J.L. Does the charm flow at RHIC? *Phys. Lett. B* **2003**, *557*, 26–32. [CrossRef]
20. Xu, N.; Xu, Z. Transverse dynamics at RHIC. *Nucl. Phys. A* **2003**, *715*, 587–590. [CrossRef]
21. Lin, Z.W.; Molnar, D. Quark coalescence and elliptic flow of charm hadrons. *Phys. Rev. C* **2003**, *68*, 044901. [CrossRef]
22. Moore, G.D.; Teaney, D. How much do heavy quarks thermalize in a heavy ion collision? *Phys. Rev. C* **2005**, *71*, 064904. [CrossRef]
23. Abelev, B.I.; Aggarwal, M.M.; Ahammed, Z.; Anderson, B.D.; Arkhipkin, D.; Averichev, G.S.; Bai, Y.; Balewski, J.; Barannikova, O.; Barnby, L.S.; et al. Measurements of phi meson production in relativistic heavy-ion collisions at RHIC. *Phys. Rev. C* **2009**, *79*, 064903. [CrossRef]

24. Adamczyk, L.; Adkins, J.K.; Agakishiev, G.; Aggarwal, M.M.; Ahammed, Z.; Alekseev, I.; Alford, J.; Aparin, A.; Arkhipkin, D.; Aschenauer, E.C.; et al. Probing parton dynamics of QCD matter with Ω and ϕ production. *Phys. Rev. C* **2016**, *93*, 021903. [CrossRef]

25. Abelev, B.B.; Adam, J.; Adamova, D.; Adare, A.M.; Aggarwal, M.M.; Rinella, G.A.; Agnello, M.; Agocs, A.G.; Agostinelli, A.; Ahammed, Z.; et al. Multi-strange baryon production at mid-rapidity in Pb-Pb collisions at $\sqrt{s_{NN}}$ = 2.76 TeV. *Phys. Lett. B* **2014**, *728*, 216–227. Erratum in Phys. Lett. B **2014**, *734*, 409–410. [CrossRef]

26. Adler, S.S.; Afanasiev, S.; Aidala, C.; Ajitanand, N.N.; Akiba, Y.; Alexander, J.; Amirikas, R.; Aphecetche, L.; Aronson, S.H.; Averbeck, R.; et al. Centrality dependence of charm production from single electrons measurement in Au + Au collisions at s(NN)**(1/2) = 200-GeV. *Phys. Rev. Lett.* **2005**, *94*, 082301. [CrossRef] [PubMed]

27. Adams, J.; Aggarwal, M.M.; Ahammed, Z.; Amonett, J.; Anderson, B.D.; Arkhipkin, D.; Averichev, G.S.; Badyal, S.K.; Bai, Y.; Balewski, J.; et al. Open charm yields in d + Au collisions at s(NN)**(1/2) = 200-GeV. *Phys. Rev. Lett.* **2005**, *94*, 062301. [CrossRef]

28. Abelev, B.; Adam, J.; Adamova, D.; Adare, A.M.; Aggarwal, M.; Rinella, G.A.; Agocs, A.G.; Agostinelli, A.; Salazar, S.A.; Ahammed, Z.; et al. Measurement of charm production at central rapidity in proton-proton collisions at $\sqrt{s}$ = 2.76 TeV. *JHEP* **2012**, *7*, 191. [CrossRef]

29. Abelev, B.; Adam, J.; Adamova, D.; Adare, A.M.; Aggarwal, M.; Rinella, G.A.; Agocs, A.G.; Agostinelli, A.; Salazar, S.A.; Ahammed, Z.; et al. Suppression of high transverse momentum D mesons in central Pb-Pb collisions at $\sqrt{s_{NN}}$ = 2.76 TeV. *JHEP* **2012**, *9*, 112. [CrossRef]

30. Adam, J.; Adamczyk, L.; Adams, J.; Adkins, K.; Agakishiev, G.; Aggarwal, M.; Ahammed, Z.; Alekseev, I.; Anderson, D.; Aoyama, R.; et al. Centrality and transverse momentum dependence of D^0-meson production at mid-rapidity in Au+Au collisions at $\sqrt{s_{NN}}$ = 200 GeV. *Phys. Rev. C* **2019**, *99*, 034908. [CrossRef]

31. Acharya, S.; Acosta, F.T.; Adamová, D.; Adolfsson, J.; Aggarwal, M.M.; Rinella, G.A.; Agnello, M.; Agrawal, N.; Ahammed, Z.; Ahn, S.U.; et al. Measurement of D^0, D^+, D^{*+} and D_s^+ production in Pb-Pb collisions at $\sqrt{s_{NN}}$ = 5.02 TeV. *JHEP* **2018**, *10*, 174. [CrossRef]

32. Radhakrishnan, S. Measurements of open charm production in Au+Au collisions at $\sqrt{s_{NN}}$ = 200 GeV with the STAR experiment at RHIC. *Nucl. Phys. A* **2019**, *982*, 659–662. [CrossRef]

33. Zhou, L. Measurements of Λ_c^+ and D_s^+ productions in Au+Au collisions at $\sqrt{s_{NN}}$ = 200 GeV from STAR. *Nucl. Phys. A* **2017**, *967*, 620–623. [CrossRef]

34. Acharya, S.; Adamová, D.; Adhya, S.P.; Adler, A.; Adolfsson, J.; Aggarwal, M.M.; Rinella, G.A.; Agnello, M.; Agrawal, N.; Ahammed, Z.; et al. Measurement of prompt D^0, D^+, D^{*+}, and D_S^+ production in p–Pb collisions at $\sqrt{s_{NN}}$ = 5.02 TeV. *JHEP* **2019**, *12*, 092. [CrossRef]

35. Acharya, S.; Acosta, F.T.; Adamova, D.; Adhya, S.P.; Adler, A.; Adolfsson, J.; Aggarwal, M.M.; Rinella, G.A.; Agnello, M.; Agrawal, N.; et al. Λ_c^+ production in Pb-Pb collisions at $\sqrt{s_{NN}}$ = 5.02 TeV. *Phys. Lett. B* **2019**, *793*, 212–223. [CrossRef]

36. Acharya, S.; Acosta, F.T.; Adamová, D.; Adolfsson, J.; Aggarwal, M.M.; Rinella, G.A.; Agnello, M.; Agrawal, N.; Ahammed, Z.; Ahn, S.U.; et al. Λ_c^+ production in pp collisions at $\sqrt{s}$ = 7 TeV and in p-Pb collisions at $\sqrt{s_{NN}}$ = 5.02 TeV. *JHEP* **2018**, *04*, 108. [CrossRef]

37. Adams, J.; Aggarwal, M.M.; Ahammed, Z.; Amonett, J.; Anderson, B.D.; Anderson, M.; Arkhipkin, D.; Averichev, G.S.; Bai, Y.; Balewski, J.; et al. Scaling Properties of Hyperon Production in Au+Au Collisions at s**(1/2) = 200-GeV. *Phys. Rev. Lett.* **2007**, *98*, 062301. [CrossRef]

38. Adams, J.; Aggarwal, M.M.; Ahammed, Z.; Amonett, J.; Anderson, B.D.; Anderson, M.; Arkhipkin, D.; Averichev, G.S.; Bai, Y.; Balewski, J.; et al. Bulk Properties of the Medium Produced in Relativistic Heavy-Ion Collisions from the Beam Energy Scan Program. *Phys. Rev. C* **2017**, *96*, 044904. [CrossRef]

39. Adam, J.; Adamczyk, L.; Adams, J.; Adkins, K.; Agakishiev, G.; Aggarwal, M.; Ahammed, Z.; Alekseev, I.; Anderson, D.; Aoyama, R.; et al. Strange hadron production in Au+Au collisions at $\sqrt{s_{NN}}$ = 7.7, 11.5, 19.6, 27, and 39 GeV. *Phys. Rev. C* **2020**, *102*, 034909. [CrossRef]

40. Acharya, S.; Adamova, D.; Adler, A.; Adolfsson, J.; Rinella, G.A.; Agnello, M.; Agrawal, N.; Ahammed, Z.; Ahmad, S.; Ahn, S.U.; et al. Production of $K^*(892)^0$ and $\phi(1020)$ in pp and Pb-Pb collisions at $\sqrt{s_{NN}}$ = 5.02 TeV. *Phys. Rev. C* **2022**, *106*, 034907. [CrossRef]

41. Abelev, B.I.; Aggarwal, M.M.; Ahammed, Z.; Anderson, B.D.; Anderson, M.; Arkhipkin, D.; Averichev, G.S.; Bai, Y.; Balewski, J.; Barannikova, O.; et al. Identified baryon and meson distributions at large transverse momenta from Au+Au collisions at s(NN)**(1/2) = 200-GeV. *Phys. Rev. Lett.* **2006**, *97*, 152301. [CrossRef]

42. Adare, A.; Afanasiev, S.; Aidala, C.; Ajitanand, N.N.; Akiba, Y.; Al-Bataineh, H.; Alexander, J.; Al-Jamel, A.; Aoki, K.; Aphecetche, L.; et al. Scaling properties of azimuthal anisotropy in Au+Au and Cu+Cu collisions at s(NN) = 200-GeV. *Phys. Rev. Lett.* **2007**, *98*, 162301. [CrossRef] [PubMed]

43. Blume, C.; Markert, C. Strange hadron production in heavy ion collisions from SPS to RHIC. *Prog. Part. Nucl. Phys.* **2011**, *66*, 834–879. [CrossRef]

44. Abelev, B.B.; Adam, J.; Adamova, D.; Aggarwal, M.M.; Rinella, G.A.; Agnello, M.; Agostinelli, A.; Agrawal, N.; Ahammed, Z.; Ahmad, N.; et al. Production of charged pions, kaons and protons at large transverse momenta in pp and Pb–Pb collisions at $\sqrt{s_{NN}}$ = 2.76 TeV. *Phys. Lett. B* **2014**, *736*, 196–207. [CrossRef]

45. Kolb, P.F.; Heinz, U.W.; Huovinen, P.; Eskola, K.J.; Tuominen, K. Centrality dependence of multiplicity, transverse energy, and elliptic flow from hydrodynamics. *Nucl. Phys. A* **2001**, *696*, 197–215. [CrossRef]

46. Shen, C.; Heinz, U.; Huovinen, P.; Song, H. Systematic parameter study of hadron spectra and elliptic flow from viscous hydrodynamic simulations of Au+Au collisions at $\sqrt{s_{NN}} = 200$ GeV. *Phys. Rev. C* **2010**, *82*, 054904. [CrossRef]

47. Andronic, A.; Braun-Munzinger, P.; Redlich, K.; Stachel, J. Charmonium and open charm production in nuclear collisions at SPS/FAIR energies and the possible influence of a hot hadronic medium. *Phys. Lett. B* **2008**, *659*, 149–155. [CrossRef]

48. Kuznetsova, I.; Rafelski, J. heavy-flavor hadrons in statistical hadronization of strangeness-rich QGP. *Eur. Phys. J. C* **2007**, *51*, 113–133. [CrossRef]

49. Andronic, A.; Arleo, F.; Arnaldi, R.; Beraudo, A.; Bruna, E.; Caffarri, D.; Valle, Z.C.D.; Contreras, J.G.; Dahms, T.; Dainese, A.; et al. Heavy-flavour and quarkonium production in the LHC era: From proton–proton to heavy-ion collisions. *Eur. Phys. J. C* **2016**, *76*, 107. [CrossRef]

50. Greco, V.; Ko, C.M.; Lévai, P. Parton coalescence and anti-proton/pion anomaly at RHIC. *Phys. Rev. Lett.* **2003**, *90*, 202302. [CrossRef]

51. Fries, R.J.; Müller, B.; Nonaka, C.; Bass, S.A. Hadronization in heavy ion collisions: Recombination and fragmentation of partons. *Phys. Rev. Lett.* **2003**, *90*, 202303. [CrossRef] [PubMed]

52. Hwa, R.C.; Yang, C.B. Scaling behavior at high p(T) and the p/pi ratio. *Phys. Rev.* **2003**, *C67*, 034902. [CrossRef]

53. Shao, F.l.; Xie, Q.b.; Wang, Q. Production rates for hadrons, pentaquarks Theta+ and Theta*++, and di-baryon (Omega Omega)(0+) in relativistic heavy ion collisions by a quark combination model. *Phys. Rev. C* **2005**, *71*, 044903. [CrossRef]

54. Greco, V.; Ko, C.M.; Rapp, R. Quark coalescence for charmed mesons in ultrarelativistic heavy ion collisions. *Phys. Lett. B* **2004**, *595*, 202–208. [CrossRef]

55. Oh, Y.; Ko, C.M.; Lee, S.H.; Yasui, S. Heavy baryon/meson ratios in relativistic heavy ion collisions. *Phys. Rev. C* **2009**, *79*, 044905. [CrossRef]

56. Liu, Y.; Greiner, C.; Kostyuk, A. B_c meson enhancement and the momentum dependence in Pb + Pb collisions at energies available at the CERN Large Hadron Collider. *Phys. Rev. C* **2013**, *87*, 014910. [CrossRef]

57. Lee, S.H.; Ohnishi, K.; Yasui, S.; Yoo, I.K.; Ko, C.M. Lambda(c) enhancement from strongly coupled quark-gluon plasma. *Phys. Rev. Lett.* **2008**, *100*, 222301. [CrossRef]

58. He, M.; Fries, R.J.; Rapp, R. Heavy-Quark Diffusion and Hadronization in Quark-Gluon Plasma. *Phys. Rev. C* **2012**, *86*, 014903. [CrossRef]

59. Plumari, S.; Minissale, V.; Das, S.K.; Coci, G.; Greco, V. Charmed Hadrons from Coalescence plus Fragmentation in relativistic nucleus-nucleus collisions at RHIC and LHC. *Eur. Phys. J. C* **2018**, *78*, 348. [CrossRef]

60. Zhao, J.; Shi, S.; Xu, N.; Zhuang, P. Sequential Coalescence with Charm Conservation in High Energy Nuclear Collisions. *arXiv* **2018**, arXiv:1805.10858.

61. Cho, S.; Sun, K.J.; Ko, C.M.; Lee, S.H.; Oh, Y. Charmed hadron production in an improved quark coalescence model. *Phys. Rev. C* **2020**, *101*, 024909. [CrossRef]

62. Wang, R.q.; Song, J.; Shao, F.l. Yield correlations and p_T dependence of charm hadrons in Pb + Pb collisions at $\sqrt{s_{NN}} = 2.76$ TeV. *Phys. Rev. C* **2015**, *91*, 014909. [CrossRef]

63. He, M.; Fries, R.J.; Rapp, R. heavy-flavor at the Large Hadron Collider in a Strong Coupling Approach. *Phys. Lett. B* **2014**, *735*, 445–450. [CrossRef]

64. Molnar, D.; Voloshin, S.A. Elliptic flow at large transverse momenta from quark coalescence. *Phys. Rev. Lett.* **2003**, *91*, 092301. [CrossRef]

65. Xie, Q.B.; Mo, W.C.; Li, Y.F. THE COMBINATION RULE OF QUARKS IN E+ E- ANNIHILATION. (IN CHINESE). *HEPNP* **1984**, *8*, 642–647.

66. Xie, Q.B.; Liu, X.M. Quark Production Rule in $e^+ e^- \to$ Two Jets. *Phys. Rev. D* **1988**, *38*, 2169–2177. [CrossRef]

67. Xie, Q.B. Quark combination rule and correlations between baryons. In Proceedings of the 19th International Symposium on Multiparticle Dynamics: New Data and Theoretical Trends, Arles, France, 13–17 June 1988.

68. Chen, C.J.; Ma, W.J.; Xie, Q.B. THE NEAREST CORRELATION IN RAPIDITY AND THE MULTIPLICITY DISTRIBUTION IN E+ E- ANNIHILATION. *J. Phys. G* **1988**, *14*, 1339–1344. [CrossRef]

69. Fang, H.P.; Xie, Q.B.; Lai, X.P. RAPIDITY DISTRIBUTION AND BARYON-ANTI-BARYON CORRELATIONS IN E+ E- —> TWO JET EVENTS. (IN CHINESE). *HEPNP* **1989**, *13*, 518–525.

70. Liang, Z.T.; Xie, Q.B. Baryon anti-baryon flavor correlations in e+ e- annihilation. *Phys. Rev. D* **1991**, *43*, 751–759. [CrossRef]

71. Shao, C.E.; Song, J.; Shao, F.L.; Xie, Q.B. Hadron production by quark combination in central Pb+Pb collisions at s(NN)**(1/2) = 17.3-GeV. *Phys. Rev.* **2009**, *C80*, 014909. [CrossRef]

72. Song, J.; Shao, F.L. Baryon-antibaryon production asymmetry in relativistic heavy ion collisions. *Phys. Rev. C* **2013**, *88*, 027901. [CrossRef]

73. Song, J.; Gou, X.R.; Shao, F.L.; Liang, Z.T. Quark number scaling of hadronic p_T spectra and constituent quark degree of freedom in p-Pb collisions at $\sqrt{s_{NN}} = 5.02$ TeV. *Phys. Lett.* **2017**, *B774*, 516–521. [CrossRef]

74. Gou, X.R.; Shao, F.L.; Wang, R.Q.; Li, H.H.; Song, J. New insights into hadron production mechanism from p_T spectra in pp collisions at $\sqrt{s} = 7$ TeV. *Phys. Rev.* **2017**, *D96*, 094010. [CrossRef]

75. Wang, R.Q.; Song, J.; Shao, F.L.; Liang, Z.T. Charmed hadron production via equal-velocity quark combination in ultrarelativistic heavy ion collisions. *Phys. Rev. C* **2020**, *101*, 054903. [CrossRef]
76. Song, J.; Shao, F.L.; Liang, Z.T. Quark number scaling of p_T spectra for Ω and ϕ in relativistic heavy-ion collisions. *Phys. Rev. C* **2020**, *102*, 014911. [CrossRef]
77. Li, H.H.; Shao, F.L.; Song, J. Production of light-flavor and single-charmed hadrons in pp collisions at $\sqrt{s} = 5.02$ TeV in an equal-velocity quark combination model. *Chin. Phys. C* **2021**, *45*, 113105. [CrossRef]
78. Song, J.; Li, H.H.; Shao, F.L. Signals of quark combination at hadronization in pp collisions at $\sqrt{s} = 200$ GeV. *Phys. Rev. D* **2022**, *105*, 074027. [CrossRef]
79. Song, J.; Li, H.H.; Shao, F.L. New feature of low p_T charm quark hadronization in *pp* collisions at $\sqrt{s} = 7$ TeV. *Eur. Phys. J. C* **2018**, *78*, 344. [CrossRef]
80. Li, H.H.; Shao, F.L.; Song, J.; Wang, R.Q. Production of single-charm hadrons by quark combination mechanism in *p*-Pb collisions at $\sqrt{s_{NN}} = 5.02$ TeV. *Phys. Rev.* **2018**, *C97*, 064915. [CrossRef]
81. Acharya, S.; Adamova, D.; Adler, A.; Adolfsson, J.; Rinella, G.A.; Agnello, M.; Agrawal, N.; Ahammed, Z.; Ahmad, S.; Ahn, S.U.; et al. Measurement of Prompt D^0, Λ_c^+, and $\Sigma_c^{0,++}(2455)$ Production in Proton–Proton Collisions at $\sqrt{s} = 13$ TeV. *Phys. Rev. Lett.* **2022**, *128*, 012001. [CrossRef]
82. First measurement of Λ_c^+ production down to $p_T = 0$ in pp and p-Pb collisions at $\sqrt{s_{NN}} = 5.02$ TeV. *arXiv* **2022**, arXiv:2211.14032.
83. Acharya, S.; Adamova, D.; Adler, A.; Adolfsson, J.; Rinella, G.A.; Agnello, M.; Agrawal, N.; Ahammed, Z.; Ahmad, S.; Ahn, S.U.; et al. Inclusive heavy-flavour production at central and forward rapidity in Xe-Xe collisions at $\sqrt{s_{NN}} = 5.44$ TeV. *Phys. Lett. B* **2021**, *819*, 136437. [CrossRef]
84. Acharya, S.; Adamová, D.; Adler, A.; Adolfsson, J.; Rinella, G.A.; Agnello, M.; Agrawal, N.; Ahammed, Z.; Ahmad, S.; Ahn, S.U.; et al. Prompt D^0, D^+, and D^{*+} production in Pb–Pb collisions at $\sqrt{s_{NN}} = 5.02$ TeV. *JHEP* **2022**, *1*, 174. [CrossRef]
85. Acharya, S.; Adamova, D.; Adler, A.; Adolfsson, J.; Rinella, G.A.; Agnello, M.; Agrawal, N.; Ahammed, Z.; Ahmad, S.; Ahn, S.U.; et al. Measurement of prompt D_s^+-meson production and azimuthal anisotropy in Pb–Pb collisions at $\sqrt{s_{NN}} = 5.02$TeV. *Phys. Lett. B* **2022**, *827*, 136986. [CrossRef]
86. Acharya, S.; Adamova, D.; Adler, A.; Adolfsson, J.; Rinella, G.A.; Agnello, M.; Agrawal, N.; Ahammed, Z.; Ahmad, S.; Ahn, S.U.; et al. Constraining hadronization mechanisms with Λ_c^+/D^0 production ratios in Pb-Pb collisions at $\sqrt{s_{NN}} = 5.02$ TeV. *arXiv* **2021**, arXiv:2112.08156.
87. Yang, Y.g.; Song, J.; Shao, F.l.; Liang, Z.t.; Wang, Q. Statistical method in quark combination model. *Chin. Phys. C* **2020**, *44*, 034103. [CrossRef]
88. Wang, Q.; Xie, Q.B. Production percentages of excited baryons in e+ e- annihilation. *J. Phys. G* **1995**, *21*, 897–904. [CrossRef]
89. Wang, R.q.; Shao, F.l.; Song, J.; Xie, Q.b.; Liang, Z.t. Hadron Yield Correlation in Combination Models in High Energy AA Collisions. *Phys. Rev. C* **2012**, *86*, 054906. [CrossRef]
90. Liang, Z.T.; Wang, X.N. Spin alignment of vector mesons in non-central A+A collisions. *Phys. Lett. B* **2005**, *629*, 20–26. [CrossRef]
91. Yang, Y.G.; Fang, R.H.; Wang, Q.; Wang, X.N. Quark coalescence model for polarized vector mesons and baryons. *Phys. Rev. C* **2018**, *97*, 034917. [CrossRef]
92. Sheng, X.L.; Oliva, L.; Wang, Q. What can we learn from the global spin alignment of ϕ mesons in heavy-ion collisions? *Phys. Rev. D* **2022**, *101*, 096005. [CrossRef]
93. Sheng, X.L.; Oliva, L.; Liang, Z.T.; Wang, Q.; Wang, X.N. Spin alignment of vector mesons in heavy-ion collisions. *arXiv* **2022**, arXiv:2205.15689.
94. Wiedemann, U.A.; Scotto, P.; Heinz, U.W. Transverse momentum dependence of Hanbury-Brown-Twiss correlation radii. *Phys. Rev. C* **1996**, *53*, 918–931. [CrossRef] [PubMed]
95. Retiere, F.; Lisa, M.A. Observable implications of geometrical and dynamical aspects of freeze out in heavy ion collisions. *Phys. Rev. C* **2004**, *70*, 044907. [CrossRef]
96. Tanabashi, M.; Hagiwara, K.; Hikasa, K.; Nakamura, K.; Sumino, Y.; Takahashi, F.; Tanaka, J.; Agashe, K.; Aielli, G.; Amsler, C.; et al. Review of Particle Physics. *Phys. Rev. D* **2018**, *98*, 030001. [CrossRef]
97. Acharya, S.; Adamova, D.; Adler, A.; Adolfsson, J.; Aggarwal, M.M.; Rinella, G.A.; Agnello, M.; Agrawal, N.; Ahammed, Z.; Ahmad, S.; et al. Evidence of rescattering effect in Pb-Pb collisions at the LHC through production of $K^*(892)^0$ and $\phi(1020)$ mesons. *Phys. Lett. B* **2020**, *802*, 135225. [CrossRef]
98. Kalinak, P. Strangeness production in Pb-Pb collisions with ALICE at the LHC. *PoS* **2017**, *EPS-HEP2017*, 168. [CrossRef]
99. Greco, V.; Ko, C.M.; Lévai, P. Parton coalescence at RHIC. *Phys. Rev. C* **2003**, *68*, 034904. [CrossRef]
100. Fries, R.J.; Muller, B.; Nonaka, C.; Bass, S.A. Hadron production in heavy ion collisions: Fragmentation and recombination from a dense parton phase. *Phys. Rev. C* **2003**, *68*, 044902. [CrossRef]
101. Scardina, F.; Das, S.K.; Minissale, V.; Plumari, S.; Greco, V. Estimating the charm quark diffusion coefficient and thermalization time from D meson spectra at energies available at the BNL Relativistic Heavy Ion Collider and the CERN Large Hadron Collider. *Phys. Rev. C* **2017**, *96*, 044905. [CrossRef]